

Probing Axions with Radiation from Magnetic Stars

Dong Lai*

Center for Radiophysics and Space Research, Department of Astronomy, Cornell University, Ithaca, NY 14853

Jeremy Heyl†

*Department of Physics and Astronomy, University of British Columbia,
Vancouver BC V6T 1Z1 Canada; Canada Research Chair*

Recent experiments suggest that polarized photons may couple significantly to pseudoscalar particles such as axions. We study the possible observational signatures of axion-photon coupling for radiation from magnetic stars, with particular focus on neutron stars. We present general methods for calculating the axion-photon conversion probability during propagation through a varying magnetized vacuum as well as across an inhomogeneous atmosphere. Partial axion-photon conversion may take place in the vacuum region outside the star. Strong axion-photon mixing occurs due to a resonance in the atmosphere, and depending on the axion coupling strength and other parameters, significant axion-photon conversion can take place at the resonance. Such conversions may produce observable effects on the radiation spectra and polarization signals from the star. We also apply our results to axion-photon propagation in the Sun and in magnetic white dwarfs.

I. INTRODUCTION

The axion is a hypothesized pseudoscalar particle arising from the breaking of a $U(1)$ Peccei-Quinn symmetry, introduced to explain the absence of strong CP violation[1, 2, 3]. The axion is also an ideal candidate for cold dark matter that makes up five-sixths of all matter in the universe. The allowed axion mass m_a is in the range of $10^{-6} \lesssim m_a \lesssim 10^{-3}$ eV[4].

A general property of the axion is that it can couple to two photons (real or virtual) via the interaction

$$\mathcal{L}_{a\gamma\gamma} = -\frac{1}{4} g a F_{\mu\nu} \tilde{F}^{\mu\nu} = g a \mathbf{E} \cdot \mathbf{B}, \quad (1)$$

where a is the axion field, $F_{\mu\nu}$ ($\tilde{F}^{\mu\nu}$) is the (dual) electromagnetic field strength tensor, and g is the photon-axion coupling constant. Accordingly, in the presence of a magnetic field \mathbf{B} , a photon may oscillate into an axion and vice versa. Exploiting such photon-axion oscillation, experiments based on “photon regeneration” (“invisible light shining through walls”) set the constraint $g < 6.7 \times 10^{-7}$ GeV $^{-1}$ (95% CL) for axions with $m_a < 10^{-3}$ eV[5]. The first results from the CERN Axion Solar Telescope (CAST) experiment imply an upper limit $g \lesssim 10^{-10}$ GeV $^{-1}$ for $m_a \lesssim 0.02$ eV [6]. Other experimental and astrophysical constraints on the axion parameters (mass m_a and g) are reviewed in Refs. [4, 7, 8].

Recently, the PVLAS collaboration has reported measurements of the rotation of the polarization of photons in passing through a vacuum cavity in a magnetic field [9]. If interpreted as due to the conversion of photons to axions, this may imply $g \simeq (1.6 - 5) \times 10^{-6}$ GeV $^{-1}$ for $m_a \sim 10^{-3}$ eV. Unfortunately, this result contradicts the

constraint from the CAST experiment and the previous energy-loss limit from globular cluster stars. Thus, either there remain systematic effects in the PVLAS experiment or nonminimal models of psuedoscalar-photon coupling are required [10].

In this paper, we study the effects of axion-photon coupling on radiation from magnetic stars (see [11] for previous works). We will consider generic axion parameters with $m_a \lesssim 10^{-3}$ eV and $g \lesssim 10^{-6}$ GeV $^{-1}$. Our goal is to understand and quantify what might be the observational signatures of axion-photon coupling for various axion parameters. Our method and basic results (such as the axion-photon conversion probability) can be applied for all axion parameters and in different astrophysical environments. Most of the paper will deal with magnetic neutron stars, for which most significant effects are possible. But we also discuss applications of our results in the contexts of magnetic white dwarfs and the Sun.

Our paper is organized as follows. In Sect. II we study axion-photon propagation in the vacuum region outside a magnetic neutron star, taking into account of the variation of the magnetic field. Section III examines the propagation in a magnetized plasma characteristic of a neutron star atmosphere. We study in detail the properties of the axion-photon resonance as the photon-axion propagates in an inhomogeneous medium. Depending on the axion coupling strength and other parameters, significant axion-photon conversion may take place and such conversion may leave an imprint on the radiation spectrum and polarization from the star. In Sect. IV we consider axion-photon propagation in the Sun and in magnetic white dwarfs, and Sect. V contains a brief discussion of our results.

*Electronic address: dong@astro.cornell.edu

†Electronic address: heyl@phas.ubc.ca

II. AXION-PHOTON PROPAGATION IN AN INHOMOGENEOUS MAGNETIZED VACUUM

Here we consider the effect of axion-photon coupling as the photon propagates radially outwards through the vacuum region outside a magnetized neutron star. The stellar magnetic field is assumed to be dipolar. Both of these assumptions are valid several radii away from the star.

A. Basic Equations

In an external static magnetic field \mathbf{B} , the evolution of the photon electric field \mathbf{E} and the axion field a of a given energy ω (so that $\mathbf{E}, a \propto e^{i\omega t}$) takes the form [11] (in units with $\hbar = c = 1$):

$$i \frac{d}{dz} \begin{pmatrix} a \\ E_{\parallel} \end{pmatrix} = \begin{pmatrix} \omega + \Delta_a & \Delta_M \\ \Delta_M & \omega + \Delta_{\parallel} \end{pmatrix} \begin{pmatrix} a \\ E_{\parallel} \end{pmatrix}, \quad (2)$$

where E_{\parallel} is the photon electric field in the plane spanned by \mathbf{B} and the z -axis, and we have assumed that the wave propagates in the z -direction. The matrix element Δ_{\parallel} arises from vacuum polarization [12, 13, 14, 15] and is given by (for $\omega \ll m_e$, the electron rest mass)

$$\Delta_{\parallel} = \frac{1}{2} q \omega \sin^2 \theta, \quad (3)$$

where θ is the angle between the direction of propagation and the magnetic field, and q is a dimensionless function of $b = B/B_Q$, with $B_Q = m_e^2 c^3 / (e\hbar) = 4.414 \times 10^{13}$ G the critical QED field strength. For $b \ll 1$, $q = 7\alpha b^2 / (45\pi)$. A general fitting formula (accurate to within 3% for all b 's) which has the correct $b \ll 1$ and $b \gg 1$ limits is [16]

$$q = \frac{7\alpha}{45\pi} b^2 \hat{q}, \quad \text{with } \hat{q} = \frac{1 + 1.2b}{1 + 1.33b + 0.56b^2}. \quad (4)$$

Thus

$$\Delta_{\parallel} = \frac{7\alpha}{90\pi} \hat{q} \beta^2 \omega = 0.1807 \hat{q} \beta^2 \omega_1 \text{ eV} = 9173 \hat{q} \beta^2 \omega_1 \text{ cm}^{-1}, \quad (5)$$

where $\omega_1 = \omega / (1 \text{ keV})$ and

$$\beta = b \sin \theta = \frac{B}{B_Q} \sin \theta. \quad (6)$$

The matrix element Δ_a in Eq. (2) is due to the finite axion mass, and Δ_M arises from the photon-axion coupling:

$$\begin{aligned} \Delta_a &= -\frac{m_a^2}{2\omega} \\ &= -0.0005 m_1^2 \omega_1^{-1} \text{ eV} = -25.38 m_1^2 \omega_1^{-1} \text{ cm}^{-1}, \end{aligned} \quad (7)$$

$$\begin{aligned} \Delta_M &= \frac{1}{2} g B \sin \theta = \frac{g m_e^2}{2} \beta \\ &= 130.6 g_1 \beta \text{ eV} = 6.627 \times 10^6 g_1 \beta \text{ cm}^{-1}, \end{aligned} \quad (8)$$

where $m_1 = m_a / (1 \text{ eV})$ and $g_1 = g / (1 \text{ GeV}^{-1})$.

Note that Eq. (2) is valid in the weak-dispersion limit, i.e., $\Delta_{\parallel}/\omega$, $|\Delta_a|/\omega$ and Δ_M/ω are all much less than unity.

In the absence of photon-axion coupling ($\Delta_M = 0$), and with $E_{\parallel}, a \propto e^{-ikz}$, we find $k/\omega = 1 + \Delta_{\parallel}/\omega$ and $1 + \Delta_a/\omega$ for photon (the parallel-mode) and axion, respectively.

B. Evolution in a Varying Magnetic Field

It is convenient to introduce the quantity Δk and the mixing angle θ_m via

$$\Delta k = 2 [(\Delta_a - \Delta_{\parallel})^2 / 4 + \Delta_M^2]^{1/2}, \quad (9)$$

and

$$\tan 2\theta_m = \frac{\Delta_M}{(\Delta_a - \Delta_{\parallel})/2} \equiv \Lambda. \quad (10)$$

Then the evolution equation (2) can be written as

$$i \frac{d}{dz} \begin{pmatrix} a \\ E_{\parallel} \end{pmatrix} = \left[\left(\omega + \frac{\Delta_{\parallel} + \Delta_a}{2} \right) \mathbf{I} + \frac{\Delta k}{2} \begin{pmatrix} \cos 2\theta_m & \sin 2\theta_m \\ \sin 2\theta_m & -\cos 2\theta_m \end{pmatrix} \right] \begin{pmatrix} a \\ E_{\parallel} \end{pmatrix}, \quad (11)$$

where \mathbf{I} is the unit 2×2 matrix.

The eigenvalues and eigenvectors of Eq. (11) are

$$k_+ = \omega + \frac{\Delta_{\parallel} + \Delta_a}{2} + \frac{\Delta k}{2}, \quad \begin{pmatrix} a \\ E_{\parallel} \end{pmatrix}_+ = \begin{pmatrix} \cos \theta_m \\ \sin \theta_m \end{pmatrix} \quad (12)$$

for the “+” mode, and

$$k_- = \omega + \frac{\Delta_{\parallel} + \Delta_a}{2} - \frac{\Delta k}{2}, \quad \begin{pmatrix} a \\ E_{\parallel} \end{pmatrix}_- = \begin{pmatrix} -\sin \theta_m \\ \cos \theta_m \end{pmatrix} \quad (13)$$

for the “-” mode.

Figure 1 shows an example of the mode eigenvalue as a function of β (with the other parameters fixed). For sufficiently large β (such that $\Delta_{\parallel} \gg \Delta_M, |\Delta_a|$), we have $\Delta k \simeq \Delta_{\parallel} - \Delta_a$, thus $k_+ = \omega + \Delta_{\parallel}$, $k_- \simeq \omega + \Delta_a$ and $\tan 2\theta_m \simeq 0$. As β decreases, $|\tan 2\theta_m|$ first increases and then decreases. For sufficiently small β (such that $|\Delta_a| \gg \Delta_M, \Delta_{\parallel}$), we again have $\Delta k \simeq \Delta_{\parallel} - \Delta_a$, $k_+ = \omega + \Delta_{\parallel}$, $k_- \simeq \omega + \Delta_a$ and $\tan 2\theta_m \simeq 0$. Thus, for both large and small β , the “+” mode always represents the axion and the “-” mode always represents the photon. Strong mixing may occur for intermediate β 's when $\tan 2\theta_m \gtrsim 1$, but there is no “level crossing”.

Consider a photon created in the large- β region of a neutron star. As the photon propagates outward to the low- β region, it may partially convert to the axion. To calculate the net conversion probability, we define the

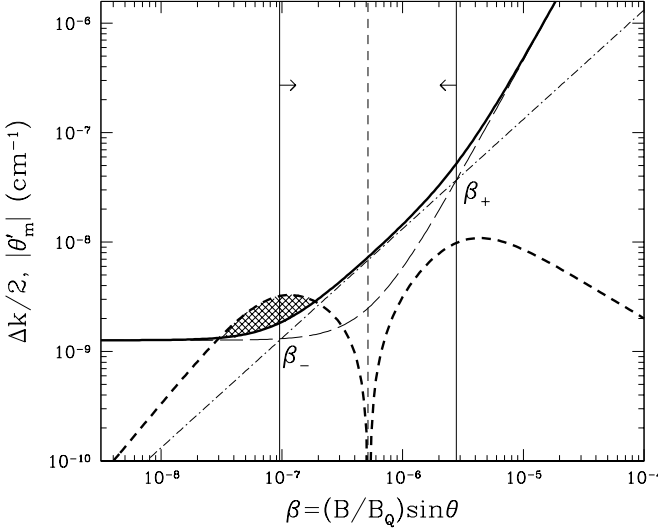


FIG. 1: The solid curve shows $\Delta k/2$, and the dashed curve shows $|\theta'_m|$ (assuming that the field is dipolar and that at the stellar surface $\beta = \beta_s = 1$ and $R = 10^6$ cm). The light dot-dashed line shows Δ_M and the long-dashed line shows $(\Delta_{\parallel} - \Delta_a)/2$. The parameters are: $m_a = 10^{-5}$ eV, $g = 2 \times 10^{-9}$ GeV $^{-1}$, $\omega = 1$ keV. The “Strong mixing” region (between the two vertical solid lines) is where $(\Delta_{\parallel} - \Delta_a)/2 < \Delta_M$ or $\beta_- < \beta < \beta_+$; nonadiabatic mode evolution occurs in the region where $\Delta k/2 < |\theta'_m|$ (cross-hatched area). The vertical dashed line denotes β_* where the maximum mixing angle is achieved.

mode amplitudes to be A_+ and A_- , and expand the photon-axion system in terms of the normal modes:

$$\begin{pmatrix} a \\ E_{\parallel} \end{pmatrix} = A_+ \begin{pmatrix} \cos \theta_m \\ \sin \theta_m \end{pmatrix} + A_- \begin{pmatrix} -\sin \theta_m \\ \cos \theta_m \end{pmatrix}. \quad (14)$$

Submitting the above in Eq. (11), we find that the mode amplitudes satisfy the equation

$$i \frac{d}{dz} \begin{pmatrix} A_+ \\ A_- \end{pmatrix} = \begin{pmatrix} \Delta k/2 & i\theta'_m \\ -i\theta'_m & -\Delta k/2 \end{pmatrix} \begin{pmatrix} A_+ \\ A_- \end{pmatrix}, \quad (15)$$

where ' denotes derivative with respect to z . In deriving Eq. (15) we have neglected the non-essential diagonal term (proportional to \mathbf{I}) in Eq. (11).

The mode evolution will be adiabatic if the condition

$$\gamma \equiv \frac{\Delta k/2}{|\theta'_m|} \gg 1 \quad (16)$$

is satisfied. From Eq. (10), we find

$$\theta'_m = \frac{\sin 4\theta_m}{4} \frac{\Lambda'}{\Lambda}, \quad \text{with} \quad \frac{\Lambda'}{\Lambda} \simeq -\frac{\beta'}{\beta} \frac{\Delta_a + \Delta_{\parallel}}{\Delta_a - \Delta_{\parallel}}, \quad (17)$$

where in the Λ'/Λ expression we have set $\dot{q}' \simeq 0$ for simplicity. For a dipolar field, we have

$$\beta \simeq \beta_s (R/r)^3, \quad (18)$$

where β_s is the field strength at the stellar surface, $R = 10^6 R_6$ cm is the NS radius. Thus $\beta'/\beta \simeq -3/r = -(3/R)(\beta/\beta_s)^{1/3}$. If the adiabatic condition (16) is satisfied at every point along the photon's path, then the photon will traverse the region of varying \mathbf{B} without any net conversion to the axion; otherwise, the photon may experience conversion and the emergent photon intensity will be smaller than the emitted intensity.

It is important to map out the parameter regimes for which net nonadiabatic photon-axion conversion may occur. To this end, we note to have any appreciable conversion, the photon must pass through a “strong mixing” region, where $|\tan 2\theta_m|$ is not much less than unity. Indeed we see from Eq. (11) that if $|\tan 2\theta_m| \ll 1$ along the photon path, then $E_{\parallel} \propto \exp(-i \int dz k_+)$ and no conversion occurs regardless of whether the condition (16) is satisfied or not. We define the “strong mixing” region by $|\tan 2\theta_m| \geq 1$, or $\beta_- \leq \beta \leq \beta_+$ (see Fig. 1), where

$$\beta_{\pm} = \frac{45\pi g m_e^2}{7\alpha\omega} \left[1 \pm \sqrt{1 - \frac{7\alpha m_a^2}{45\pi(g m_e^2)^2}} \right]. \quad (19)$$

In the above equation, we have used $\dot{q} = 1$ since for the parameters regime of interest, $\beta_{\pm} \ll 1$ is well satisfied. Thus the “strong mixing” region exists only when

$$\frac{g m_e^2}{m_a} \geq \left(\frac{g m_e^2}{m_a} \right)_* = \left(\frac{7\alpha}{45\pi} \right)^{1/2},$$

$$\text{or} \quad \frac{g_1}{m_1} \geq \left(\frac{g_1}{m_1} \right)_* = 7.28 \times 10^{-5}. \quad (20)$$

At the threshold point, β_{\pm} collapse to

$$\beta_* = \frac{m_a}{\omega} \sqrt{\frac{45\pi}{7\alpha}} = 52.6 \frac{m_a}{\omega} = 0.0526 m_1/\omega_1, \quad (21)$$

and $(\Delta k/2)_* = m_a^2/(\sqrt{2}\omega)$.

In general (not only at the threshold point) the maximum mixing angle occurs where $\beta = \beta_*$ and has the value

$$|\tan 2\theta_m|_{\max} = \frac{g_1}{m_1} \left(\frac{g_1}{m_1} \right)_*^{-1} \quad (22)$$

Suppose $g/m_a > (g/m_a)_*$, then the region where the adiabatic condition (16) is most likely to be violated is around $\beta = \beta_{\pm}$, where $|\theta_m| = \pi/8$ and $|\sin 4\theta_m| = 1$ (see Fig. 1). First consider the the parameter regime $g/m_a \gg (g/m_a)_*$. In this case, β_+ is determined by $\Delta_M \simeq \Delta_{\parallel}/2 \gg |\Delta_a|$, which gives $\beta_+ \simeq 90\pi g m_e^2/(7\alpha\omega)$. The nonadiabaticity condition $\Delta k/2 < |\theta'_m|$ at $\beta = \beta_+$ then translates to

$$g_1 < 7.55 \times 10^{-10} (\omega_1^2 \beta_s^{-1} R_6^{-3})^{1/5}. \quad (23)$$

At $\beta = \beta_-$, which is determined by $\Delta_M \simeq |\Delta_a/2| \gg |\Delta_{\parallel}|$, giving $\beta_- \simeq m_a^3/(2\omega g m_e^2) = 1.9 \times 10^{-6} m_1^2 g_1^{-1} \omega_1^{-1}$, the nonadiabaticity condition $\Delta k/2 < |\theta'_m|$ translates to

$$g_1 < 1.4 \times 10^{-28} m_1^{-4} (\omega_1^2 \beta_s^{-1} R_6^{-3}). \quad (24)$$

Figure 2 illustrates the parameter domain for which nonadiabatic photon-axion conversion may be possible.

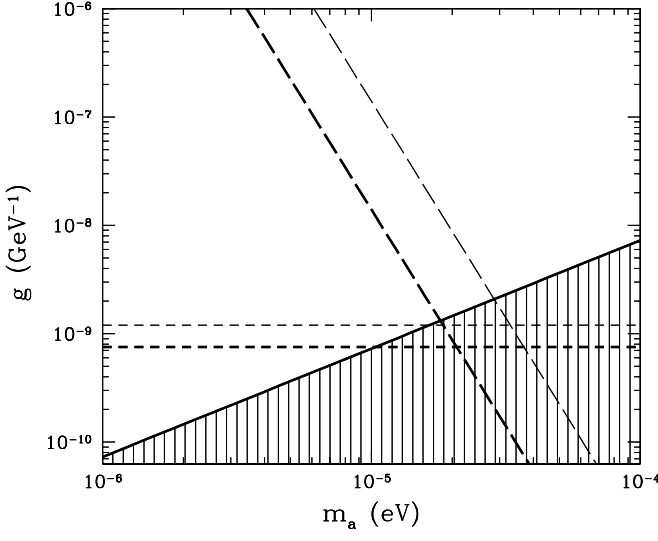


FIG. 2: The parameter domain for which nonadiabatic photon-axion conversion is possible. Above the solid line [Eq. (20)] (the unshaded regime), there exists a “strong mixing” zone ($|\tan 2\theta_m| > 1$) between photons and axions. In the unshaded region, we have $g_1/m_1 > (g_1/m_1)_*$, and well inside the unshaded region the asymptotic results of Eqs. (23) and (II C) apply. In this (unshaded) region and below the long-dashed line, mode evolution is nonadiabatic at $\beta = \beta_-$ [Eq. (II C)]; below the short-dashed line, the evolution also becomes nonadiabatic at $\beta = \beta_+$ [Eq. (23)]. The heavy lines are for $f = \omega_1^2 \beta_s^{-1} R_6^{-3} = 1$, and lighter lines for $f = 10$.

C. Numerical Calculations of Photon-Axion Conversion Probability

To obtain the photon-axion conversion probability, it is necessary to perform numerical calculations. To this end, we rewrite Eq. (15) as

$$i \frac{d}{d \ln \beta} \begin{pmatrix} A_+ \\ A_- \end{pmatrix} = \begin{pmatrix} C & iD \\ -iD & -C \end{pmatrix} \begin{pmatrix} A_+ \\ A_- \end{pmatrix}, \quad (25)$$

where

$$C = \frac{\Delta k}{2} \frac{dr}{d \ln \beta}, \quad D = \frac{d\theta_m}{d \ln \beta}. \quad (26)$$

At large β , we consider a pure photon state, with $A_- = 1$ and $A_+ = 0$. We integrate Eq. (25) toward small β and obtain the asymptotic $A_+(\beta \rightarrow 0)$, and the net conversion probability is then $P_{\text{conv}} = |A_+|^2$.

Figures 3-6 give several examples of our numerical integrations. Figures 3-5 consider the regime $(g/m_a) > (g/m_a)_*$. At low energy (Fig. 5), the mode does not evolve through a nonadiabatic zone [neither (23) nor (II C) are satisfied], thus the mode conversion probability is small. At intermediate energy (Fig. 3), the condition (II C) is satisfied while (23) is not, we obtain a large P_{conv} . At large energy (Fig. 4), both (II C) and (23) are satisfied, and yet the net conversion probability is small. Fig. 4 gives some hints as to what is happening.

When the wave travels through a non-adiabatic zone, the amplitudes of the modes change. There can be two non-adiabatic zones, one near β_+ and one near β_- . However, the sign of θ'_m is different in these two zones; therefore, the sign of the mixing term D in Eq. (25) differs as well. When both zones are active (as for $\omega = 20$ keV in Fig. 4), some of the changes in the inner zone (β_+) are undone in the outer zone (β_-). With this in mind, the peak conversion as a function of energy ω should occur approximately where Eq. (23) holds but Eq. (20) breaks down, so that the non-adiabatic region around β_- is as large as possible without the region around β_+ being non-adiabatic as well. Thus, for a given axion parameters g, m_a satisfying Eq. (20), the maximum conversion occurs for the photon energy between

$$\omega_1 \sim 0.3 \left(\frac{g}{10^{-9} \text{ GeV}^{-1}} \right)^{1/2} \left(\frac{m_a}{10^{-5} \text{ eV}} \right)^2 (\beta_s R_6^3)^{1/2} \text{ keV} \quad (27)$$

and

$$\omega_2 \sim 2 \left(\frac{g}{10^{-9} \text{ GeV}^{-1}} \right)^{5/2} (\beta_s R_6^3)^{1/2} \text{ keV}. \quad (28)$$

This nonmonotonic behavior of P_{conv} is shown in Fig. 7. As noted before, for $(g/m_a) < (g/m_a)_*$, no “strong mixing” region exists in the photon’s path, the net conversion probability will be small, regardless of whether condition (16) is satisfied or not (see Fig. 6).

D. Effect on Radiation Spectrum and Polarization from Magnetic Neutron Stars

To illustrate the effect of photon-axion coupling on the radiation from magnetized neutron stars (NSs), we consider an example of a NS with surface magnetic field $B = 10^{13}$ G and surface temperature $T_s = 0.5$ keV (see Fig. 8). As shown in Refs. [17, 18], due to the vacuum resonance effect [19, 20] occurring near the NS surface (but outside the photosphere) (see also Sect. III below), the surface radiation from such a NS is dominated by the extraordinary mode (or \perp mode) for $\omega \lesssim 1 - 2$ keV and by the ordinary mode (\parallel mode) for $\omega \gtrsim 1 - 2$ keV. In our calculation leading to Fig. 8, we assume (for simplicity) that the total intensity near the NS surface is given by a blackbody with temperature T_s (see, e.g., [18, 21] for more accurate atmosphere model spectra), and we calculate the intensities of the two photon modes (I_\perp and I_\parallel) outside the vacuum resonance layer using the method described in [19]. With no photon-axion coupling, the observed photon intensity is $I_\perp + I_\parallel$, and Stokes parameter Q is $I_\perp - I_\parallel$ (Note that the Stokes parameter depends on the orientation of the axis used in measuring linear polarization, but one can always choose the appropriate axis so that $U = 0$; Refs. [17, 18] give a more detailed description of the phase-dependent polarization signals). With nonzero photon-axion coupling, as the photon propagates

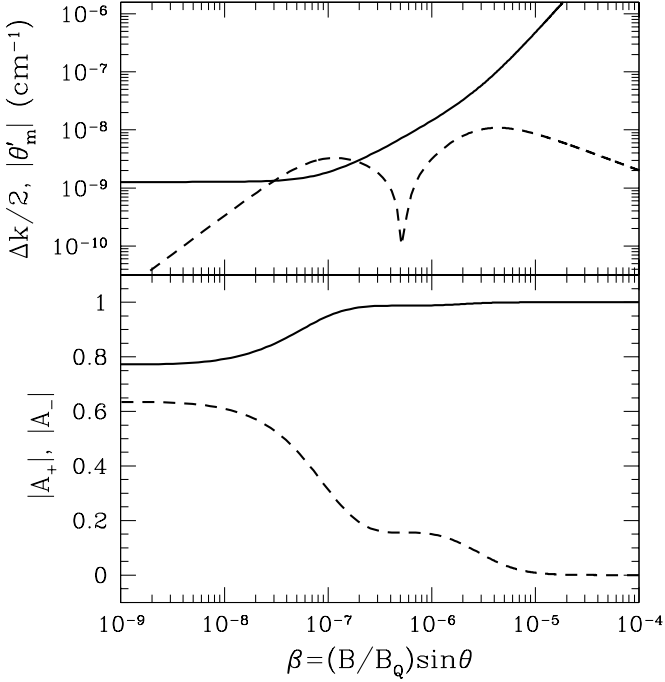


FIG. 3: The upper panel shows $\Delta k/2$ (solid line) and $|\theta'_m|$ (dashed line), similar to Fig. 1. The lower panel shows the evolution of mode amplitude, starting from $A_- = 1$, $A_+ = 0$ at a small radius (large β). The parameters are $m_a = 10^{-5}$ eV, $g = 2 \times 10^{-9}$ GeV $^{-1}$, $\omega = 1$ keV, $\beta_s = 1$, and $R_6 = 1$.

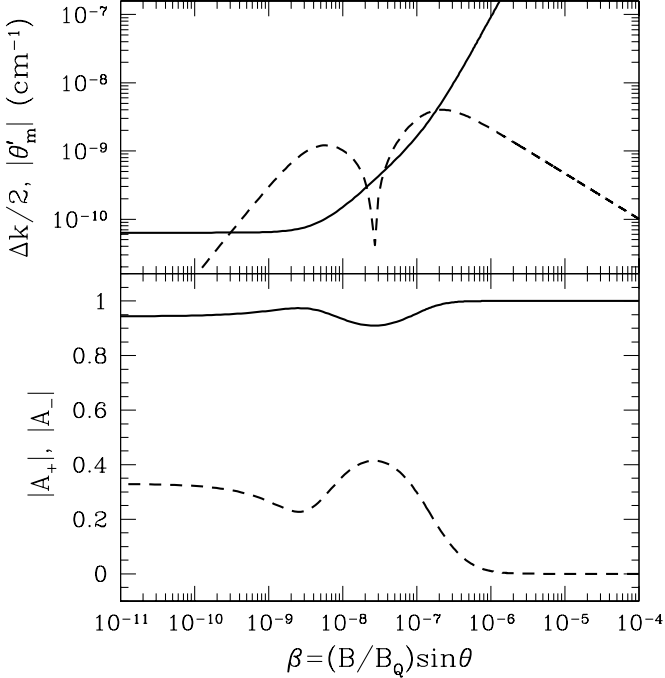


FIG. 4: Same as Fig. 3 except $\omega = 20$ keV.

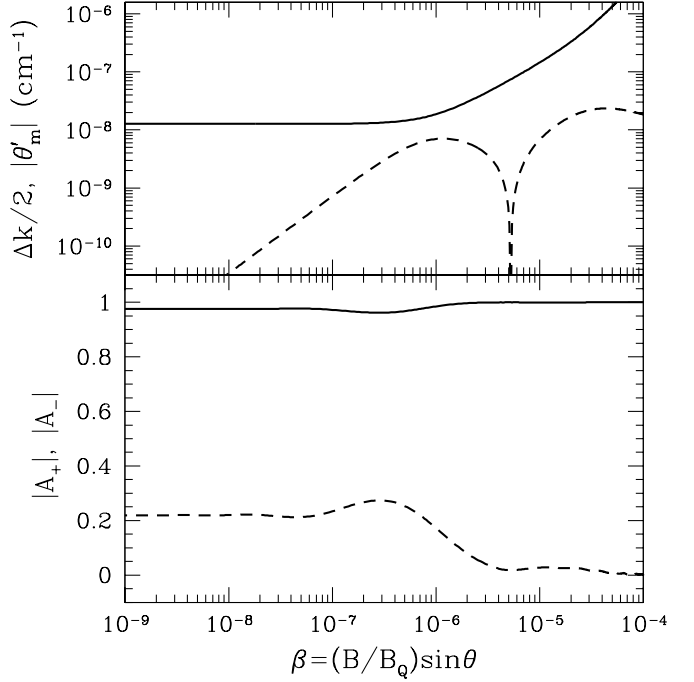


FIG. 5: Same as Fig. 3 except $\omega = 0.1$ keV.

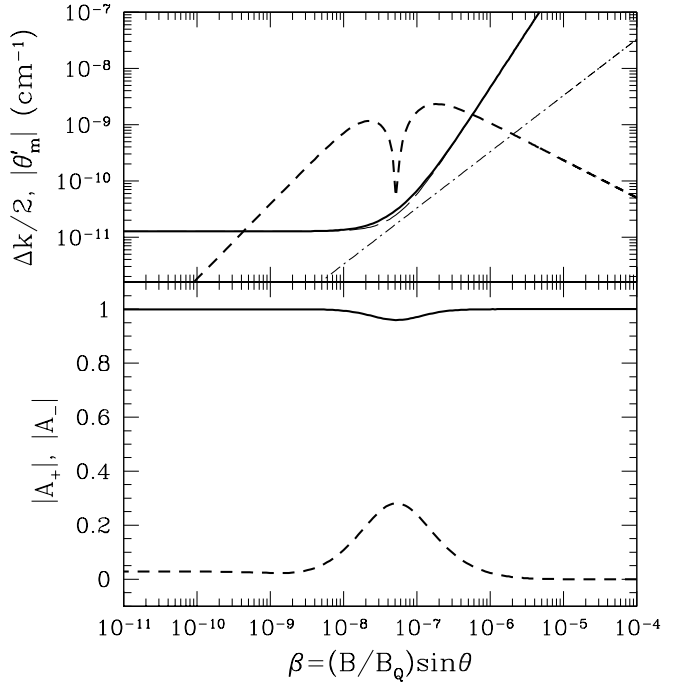


FIG. 6: Same as Fig. 3 except $m_a = 10^{-6}$ eV, $g = 5 \times 10^{-11}$ GeV $^{-1}$, $\omega = 1$ keV, $\beta_s = 1$, and $R_6 = 1$. In the upper panel, the light dot-dashed line shows Δ_M and the long-dashed line shows $(\Delta_{\parallel} - \Delta_a)/2$. Unlike the cases shown in Figs. (3)-(5), no “strong mixing” region exists in this case.

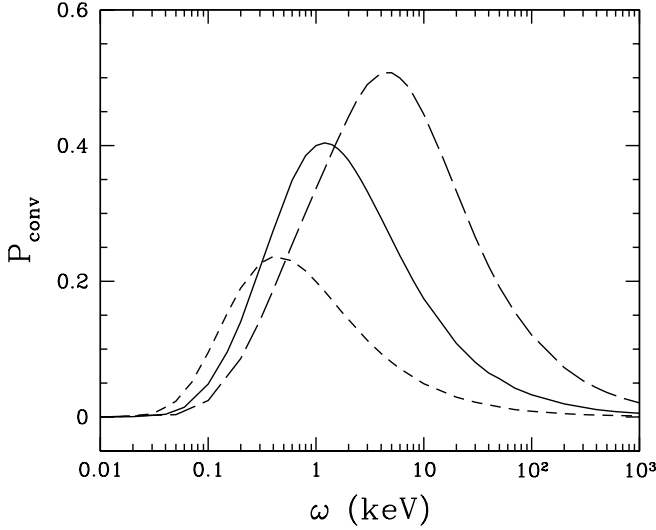


FIG. 7: Photon-axion conversion probability P_{conv} in vacuum as a function of photon energy. The parameters are $m_a = 10^{-5}$ eV, $\beta_s = 1$, $R_6 = 1$; the solid line is for $g = 2 \times 10^{-9}$ GeV $^{-1}$, the short-dashed line for $g = 10^{-9}$ GeV $^{-1}$, and the long-dashed line for $g = 4 \times 10^{-9}$ GeV $^{-1}$.

from the stellar surface to the observer, the \parallel -mode intensity will be reduced to $I_{\parallel}^{\infty} = (1 - P_{\text{conv}})I_{\parallel}$, where P_{conv} is the photon-axion conversion probability calculated before (Fig. 7), while the \perp -mode intensity is unchanged. Thus the observed total radiation intensity is $I_{\perp} + I_{\parallel}^{\infty}$, and the Stokes Q parameter is $I_{\perp} - I_{\parallel}^{\infty}$.

For NSs with $B_s \gtrsim 7 \times 10^{14}$ G, the radiation from the NS surface is dominated by the \perp -mode, which is unaffected by any further photon-axion coupling as the photon propagates to the observer. Thus, for such NSs, the axion would have a much smaller effect on the observed NS radiation than depicted in Fig. 8.

III. AXION-PHOTON PROPAGATION IN AN INHOMOGENEOUS PLASMA

In this section we consider the effect of photon-axion coupling on the photon propagation in the atmospheric plasma of a magnetized NS. Here the magnetic field is constant, but the plasma density varies on the scale of centimeters (the atmosphere scale height at $T_s \sim 10^6$ K).

A. Vacuum resonance

We first consider wave propagation in a magnetized plasma, including the vacuum polarization effect, but neglecting axion-photon coupling [17, 19, 20, 22, 23, 24]. In the weak-dispersion approximation (i.e., the index of refraction of the photon is very close to unity), the electromagnetic wave equation in the plasma including vacuum polarization (but no axion) is given by Eq.(30) of

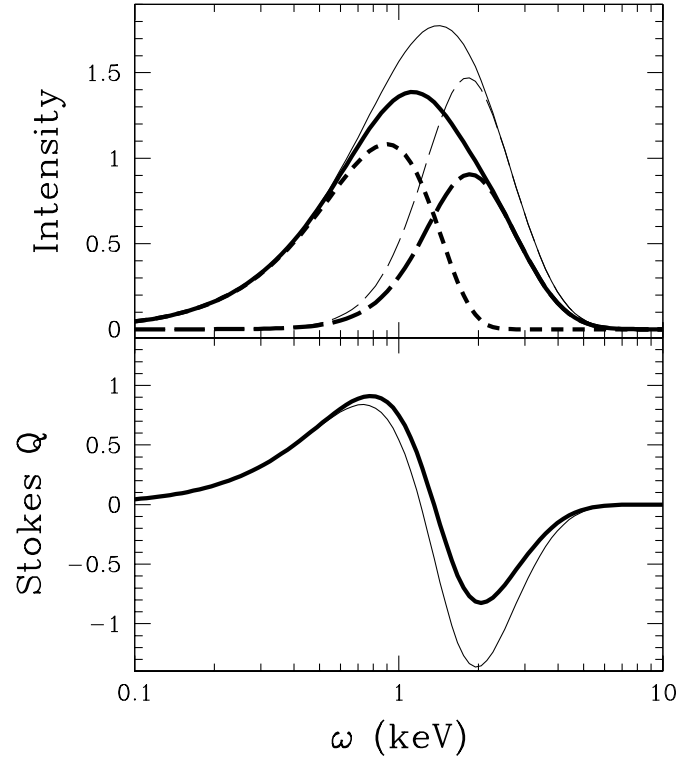


FIG. 8: Spectrum (upper panel) and Stokes parameter Q (lower panel) of a magnetized NS with surface magnetic field $B_s = 10^{13}$ G and temperature $T_s = 0.5$ keV. In both panels, the heavy lines show the results including photon-axion coupling with the parameters $m_a = 10^{-5}$ eV and $g = 2 \times 10^{-9}$ GeV $^{-1}$, while the light lines neglect photon-axion coupling. In the upper panel, the solid lines show the total radiation intensity, the short-dashed line shows the \perp -mode intensity and the long-dashed line shows the \parallel -mode intensity.

[17]. Using the sign convention adopted for this paper, we have

$$i \frac{d}{dz} \begin{pmatrix} E_{\parallel} \\ E_{\perp} \end{pmatrix} = \frac{\omega}{2} \begin{pmatrix} 2 + \sigma_{11} & \sigma_{12} \\ \sigma_{21} & 2 + \sigma_{22} \end{pmatrix} \begin{pmatrix} E_{\parallel} \\ E_{\perp} \end{pmatrix}. \quad (29)$$

Neglecting the protons (i.e. setting the proton mass $m_p \rightarrow \infty$) and damping terms in the dielectric tensors (more general expressions are given in [17]), the matrix elements are given by

$$\sigma_{11} = (q - v_e) \sin^2 \theta - \frac{v_e}{1 - u_e} \cos^2 \theta, \quad (30)$$

$$\sigma_{22} = -m \sin^2 \theta - \frac{v_e}{1 - u_e}, \quad (31)$$

$$\sigma_{12} = -\sigma_{21} = i \frac{v_e u_e^{1/2}}{1 - u_e} \cos \theta. \quad (32)$$

Here $u_e = \omega_e^2/\omega^2$, with $\omega_e = eB/(m_e c) = m_e c^2 b$ the electron cyclotron (angular) frequency, and $v_e = \omega_{pe}^2/\omega^2$, with $\omega_{pe} = (4\pi n_e e^2/m_e)^{1/2} = 28.71 (Y_e \rho_1)^{1/2}$ eV the electron plasma (angular) frequency, where $n_e = Y_e \rho/m_p$

is the electron density, ρ is the mass density, Y_e is the electron fraction and $\rho_1 = \rho/(1 \text{ g cm}^{-3})$. The quantities q, m are the vacuum polarization parameters: q is given by Eq. (4) and [16]

$$m = -\frac{4\alpha}{45\pi} b^2 \hat{m}, \quad \hat{m} = \frac{1}{1 + 0.72b^{5/4} + (4/15)b^2}. \quad (33)$$

The weak-dispersion approximation adopted in Eq. (29) is valid for $v_e \ll 1$ and $b \ll 3\pi/\alpha \sim 10^3$.

With $E_{\parallel, \perp} \propto e^{-ikz}$, Eq. (29) determines two normal modes. For $u_e \gg 1$, the modes are almost linearly polarized, except at the “vacuum resonance” [19, 20, 22, 23, 24], which occurs at $\sigma_{11} = \sigma_{22}$, or

$$v_e = (q + m) \frac{u_e - 1}{u_e}, \quad (34)$$

which for $u_e \gg 1$, becomes $v_e = q + m$. For a given photon energy, the resonance density is

$$\rho_{\text{res}}(\text{vacuum}) = 0.964 Y_e^{-1} (B_{14} \omega_1)^2 f_B^{-2} \text{ g cm}^{-3}, \quad (35)$$

where $B_{14} = B/(10^{14} \text{ G})$, $\omega_1 = \omega/(1 \text{ keV})$, and $f_B = [(\alpha b^2/15\pi)/(q+m)]^{1/2}$ is a slow varying function of B and is of order unity ($f_B \simeq 1$ for $b \lesssim 1$ and $f_B \lesssim 4$ for $b \lesssim 100$; we will use $f_B = 1$ in remainder of this paper). At the vacuum resonance, the plasma and vacuum polarization effects are comparable, and both modes are circularly polarized.

The evolution of photon modes around the vacuum resonance in an inhomogeneous NS atmosphere (varying density but constant magnetic field) has been studied before [17, 19]. The key result is that away from the resonance, the mode evolution is highly adiabatic. At the resonance, the mode evolution depends on the adiabaticity parameter

$$\gamma_{\text{res}} = (\omega/\omega_{\text{ad}})^3, \quad (36)$$

with

$$\omega_{\text{ad}} = 2.55 (f_B \tan \theta)^{2/3} H_1^{-1/3} \text{ keV}, \quad (37)$$

where $H = \rho/|\rho'|$ is the density scale height along the ray (evaluated at the resonance point), and $H_1 = H/(1 \text{ cm})$. For an ionized hydrogen atmosphere, $H = \rho/|\rho'| = 2kT/(m_p g \cos \theta_{kg}) = 1.65 T_6/(g_{14} \cos \theta_{kg}) \text{ cm}$, where $T = 10^6 T_6$ is the temperature, $g = 10^{14} g_{14} \text{ cm s}^{-2}$ is the gravitational acceleration, and θ_{kg} is the angle between the ray and the NS surface normal. Since nonadiabaticity can only occur at the vacuum resonance, we can use the Landau-Zener formula to calculate the nonadiabatic jump probability between normal modes:

$$P_{\text{jump}} = e^{-\pi \gamma_{\text{res}}/2}. \quad (38)$$

Thus, for $\gamma_{\text{res}} \gg 1$, the evolution is adiabatic, and the photon can convert from the \parallel -mode (ordinary mode) to the \perp -mode (extraordinary mode) and vice versa. Various implications of the vacuum resonance phenomenon for NS surface radiation spectrum and polarization are studied in Refs. [17, 18, 19, 20, 21].

B. Axion-Photon Resonance

We now consider the effect of photon-axion coupling on photon propagation in an inhomogeneous magnetized plasma. Combining Eqs. (2) and (29), we find that in the weak-dispersion approximation, the evolution equation for the photon (with two polarization components, E_{\parallel} and E_{\perp}) and axion takes the form

$$i \frac{d}{dz} \Phi = \begin{pmatrix} \omega + \Delta_a & \Delta_M & 0 \\ \Delta_M & \omega + \Delta_{\parallel} + \Delta_p & \sigma_{12}\omega/2 \\ 0 & \sigma_{21}\omega/2 & \omega + \sigma_{22}\omega/2 \end{pmatrix} \Phi, \quad (39)$$

where

$$\Phi = \begin{pmatrix} a \\ E_{\parallel} \\ E_{\perp} \end{pmatrix}. \quad (40)$$

In Eq. (39), Δ_a , Δ_{\parallel} and Δ_M are the same as in Eq. (2), σ_{22} , σ_{12} , σ_{21} are given by Eqs. (31)-(32), and

$$\Delta_p = -\frac{\omega v_e}{2} F, \quad \text{with} \quad F = \frac{\cos^2 \theta}{1 - u_e} + \sin^2 \theta. \quad (41)$$

Obviously, in vacuum ($v_e = 0$), Eq. (39) reduces to Eq. (2); with no photon-axion coupling ($\Delta_M = 0$), it reduces to Eq. (29).

The *axion-photon resonance* occurs when the first and second diagonal matrix elements in Eq. (39) are equal, i.e., $\Delta_a = \Delta_{\parallel} + \Delta_p$, or

$$v_e = \frac{q \sin^2 \theta + (m_a^2/\omega^2)}{F} \quad (\text{axion-photon resonance}). \quad (42)$$

Equations (39)-(42) are general, and are valid for different magnetic field regimes, such as those found in NSs, white dwarfs and the Sun.

We now consider magnetic field strengths relevant to NSs and assume $u_e \gg 1$. We consider a typical angle θ that is not too close to 0° or 180° . For the parameters (axion mass, photon energy and field strength) of interest, $q \sin^2 \theta \gg m_a^2/\omega^2$ (or $\Delta_{\parallel} \gg |\Delta_a|$) is well satisfied. Then the axion-photon resonance is at

$$v_e = q \quad (\text{axion-photon resonance}). \quad (43)$$

Note that the vacuum resonance is at $v_e = q + m$. The two resonances are well separated, and we can treat them independently — we justify this in Sect. III C.

The vacuum resonance has been discussed in Sect. III A. We now consider the axion-photon resonance. Neglecting the E_{\perp} component of the photon, the basic equation takes the form

$$i \frac{d}{dz} \begin{pmatrix} a \\ E_{\parallel} \end{pmatrix} = \begin{pmatrix} \omega + \Delta_a & \Delta_M \\ \Delta_M & \omega + \Delta_{\parallel} + \Delta_p \end{pmatrix} \begin{pmatrix} a \\ E_{\parallel} \end{pmatrix}. \quad (44)$$

Similar to Eqs. (9) and (10), we define Δk and the mixing angle θ_m via

$$\Delta k = 2 [(\Delta_a - \Delta_{\parallel} - \Delta_p)^2/4 + \Delta_M^2]^{1/2}, \quad (45)$$

$$\tan 2\theta_m = \frac{\Delta_M}{(\Delta_a - \Delta_{\parallel} - \Delta_p)/2}. \quad (46)$$

The eigenvalues and eigenvectors of Eq. (44) are

$$k_{\pm} = \omega + \frac{\Delta_{\parallel} + \Delta_a + \Delta_p}{2} \pm \frac{\Delta k}{2}, \quad (47)$$

$$\begin{pmatrix} a \\ E_{\parallel} \end{pmatrix}_+ = \begin{pmatrix} \cos \theta_m \\ \sin \theta_m \end{pmatrix}, \quad \begin{pmatrix} a \\ E_{\parallel} \end{pmatrix}_- = \begin{pmatrix} -\sin \theta_m \\ \cos \theta_m \end{pmatrix}. \quad (48)$$

If we plot k_{\pm} as a function of the plasma density, we find the two eigenstates tend to “cross” at $\Delta_a = \Delta_{\parallel} + \Delta_p$, where $\theta_m = \pm 45^\circ$ — this is the axion-photon resonance. Similar to Sect. II B, we find that the mode evolution depends on the adiabaticity ratio $\gamma = \Delta k/(2|\theta_m|)$. Assuming that the variation comes only from density (while the magnetic field is constant), we have

$$\theta'_m = \frac{\Delta_p}{4\Delta_M} \frac{\rho'}{\rho} \sin^2 2\theta_m, \quad (49)$$

Thus the adiabaticity ratio is

$$\begin{aligned} \gamma &= \left| \frac{\Delta k/2}{\theta'_m} \right| = \frac{4\Delta_M^2 H}{|\Delta_p \sin^3 2\theta_m|} \\ &= \frac{4\Delta_M^2 H}{\Delta_{\parallel}} \frac{\rho_{\text{res}}/\rho}{|\sin^3 2\theta_m|}, \end{aligned} \quad (50)$$

where in the last equality we have used $\Delta_{\parallel} \gg |\Delta_a|$, and ρ_{res} is the axion-photon resonance density (for a given photon energy ω):

$$\rho_{\text{res}} = 2.25 Y_e^{-1} (B_{14} \omega_1)^2 \hat{q} \text{ g cm}^{-3}. \quad (51)$$

At the axion-photon resonance $\rho = \rho_{\text{res}}$, $|\theta_m| = \pi/4$, we find

$$\gamma_{\text{res}} = \frac{4\Delta_M^2 H}{\Delta_{\parallel}} = 0.01915 \frac{g_{-6}^2 H_1}{\omega_1 \hat{q}}, \quad (52)$$

where $g_{-6} = g/(10^{-6} \text{ GeV}^{-1})$. Note that

$$\sin 2\theta_m = \frac{M}{[(1 - v_e/q)^2 \sin^4 \theta/16 + M^2]^{1/2}}, \quad (53)$$

with

$$M = \frac{\Delta_M}{\omega q} = 3.614 \times 10^{-4} \frac{g_{-6} \sin \theta}{b \omega_1 \hat{q}}. \quad (54)$$

For $|1 - v_e/q| \gg 4M/\sin^2 \theta$, we have

$$\gamma \simeq 6.34 \times 10^6 \frac{H_1 b^3 \omega_1^2 \hat{q}^2 \sin^3 \theta}{g_{-6}} \frac{(1 - v_e/q)^3}{v_e/q}. \quad (55)$$

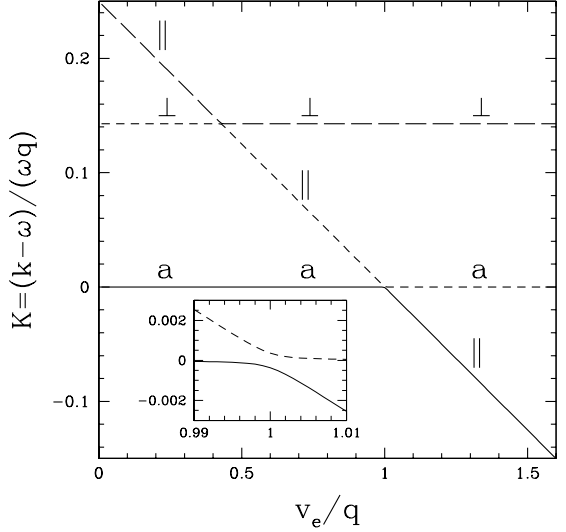


FIG. 9: Eigenvalues of the axion-photon system in the plasma+vacuum medium as a function of the plasma density parameter $V = v_e/q$, where $v_e = (\omega_{pe}/\omega)^2 \propto \rho$. The insert shows the blowup of the region around the axion-photon resonance. The parameters are chosen so that $A, M, u_e^{-1/2} \ll 1$.

Thus, away from the resonance, the adiabatic condition ($\gamma \gg 1$) is well satisfied, and nonadiabaticity can only occur very close to the resonance. We can use the Landau-Zener formula to calculate the nonadiabatic jump probability

$$P_{\text{jump}} = e^{-\pi \gamma_{\text{res}}/2}. \quad (56)$$

Note that because of the level crossing, adiabatic mode evolution ($\gamma_{\text{res}} \gg 1$) corresponds to a conversion of the \parallel -mode photon to the axion and vice versa. Thus the axion-photon conversion probability across the resonance is $P_{\text{conv}} = 1 - P_{\text{jump}}$.

Comparing Eqs. (36)-(37) with Eq. (52), it is interesting to note that high-energy photons tend to be more adiabatic at the vacuum resonance and but less adiabatic at the axion-photon resonance than low-energy photons.

In Sect. III D we shall present numerical calculations that confirm the analytical consideration given above.

C. More Rigorous Treatment of Three-State Mixing

Here we consider the eigenmodes of the three-state system, Eq. (39). We will show that the vacuum resonance and the axion-photon resonance can be considered independently of each other.

The 3×3 matrix in Eq. (39) can be written as (for $u_e \gg 1$)

$$\omega \mathbf{I} + \omega q \mathbf{G}, \quad (57)$$

where \mathbf{I} is the unit 3×3 unit matrix, and

$$\mathbf{G} = \begin{bmatrix} A & M & 0 \\ M & \frac{1}{2}(1-V)\sin^2\theta & -iV\cos\theta/(2u_e^{1/2}) \\ 0 & iV\cos\theta/(2u_e^{1/2}) & (2\hat{m}/7\hat{q})\sin^2\theta \end{bmatrix}, \quad (58)$$

with

$$V \equiv v_e/q, \quad (59)$$

$$A \equiv \Delta_a/(\omega q) \ll 1, \quad (60)$$

$$M \equiv \Delta_M/(\omega q) = 3.614 \times 10^{-4} \frac{g_{-6} \sin\theta}{b\omega_1 \hat{q}} \ll 1. \quad (61)$$

Let $(a, E_{\parallel}, E_{\perp}) \propto e^{-ikz}$, and we define dimensionless K via

$$k = \omega + \omega q K. \quad (62)$$

Obviously, K depends only on the dimensionless parameters, V , A , M , u_e . Numerical values for K as a function of V are shown in Fig. 9.

Since $M \ll 1$, $u_e^{-1/2} \ll 1$, it is clear that away from the two resonances, the eigenvalues are simply

$$K = A \quad (\text{axion}), \quad (63)$$

$$K = (1/2)(1-V)\sin^2\theta \quad (\parallel\text{-mode}), \quad (64)$$

$$K = (2\hat{m}/7\hat{q})\sin^2\theta \quad (\perp\text{-mode}). \quad (65)$$

We now consider the mode properties in the vicinity of the axion-photon resonance, $|V - 1| \ll 1$. The third eigenvalue is simply $K = (2\hat{m}/7\hat{q})\sin^2\theta$, describing the \perp -mode of photon. The other two modes that “intersect” have eigenvalues that satisfy $|K_{\pm}| \ll 1$, and are given by

$$K_{\pm} = \frac{A - C}{2} + \frac{1 - V}{4}\sin^2\theta \pm \frac{1}{4}[(V_{ap} - V)^2 \sin^4\theta + (4M)^2]^{1/2}, \quad (66)$$

where

$$C \simeq \frac{7\hat{q}}{8\hat{m}u_e \tan^2\theta} \ll 1, \quad (67)$$

and V_{ap} is the value of V at which the axion-photon resonance occurs:

$$V_{ap} = 1 - \frac{2(A + C)}{\sin^2\theta}. \quad (68)$$

Note that if we set $C = 0$, Eq. (68) reduces to Eq. (42). We see that effect of including the coupling with third mode (the \perp -mode) is to shift the axion-photon resonance location by a small amount. The eigenvectors near the resonance are

$$\Phi_+ \propto \begin{pmatrix} \cos\theta_m \\ \sin\theta_m \\ E_{\perp+} \end{pmatrix}, \quad \Phi_- \propto \begin{pmatrix} -\sin\theta_m \\ \cos\theta_m \\ E_{\perp-} \end{pmatrix}, \quad (69)$$

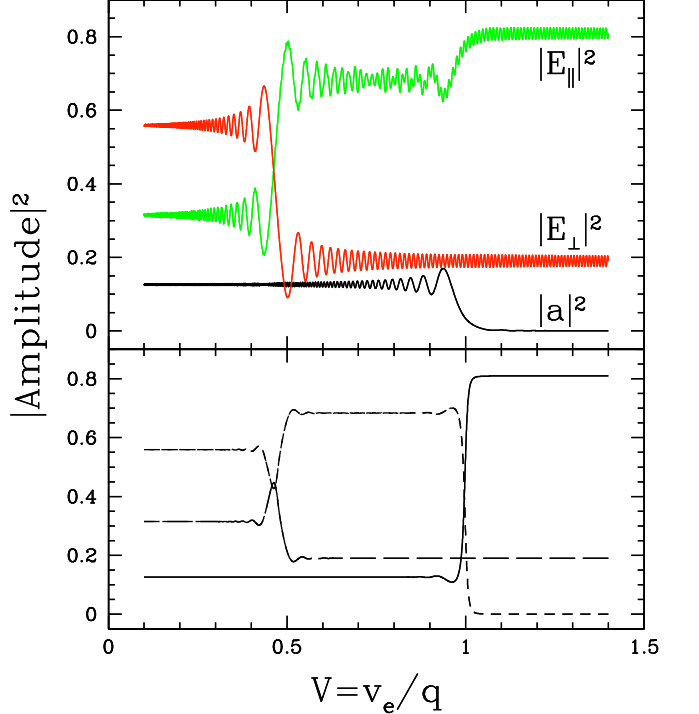


FIG. 10: The evolution of the three-state system in an inhomogeneous neutron star atmosphere. The upper panel shows the square amplitudes $|a|^2$, $|E_{\parallel}|^2$ and $|E_{\perp}|^2$; the lower panel shows the square amplitude of non-crossing eigenmodes, $|A_1|^2$, $|A_2|^2$, $|A_3|^3$. The evolution starts in the high-density (large $v_e = \omega_e^2/\omega^2$) region, where amplitudes are set to $E_{\parallel} = 0.9$, $E_{\perp} = \sqrt{0.19}$ and $a = 0$. The parameters are $m_a = 10^{-3}$ eV, $g = 10^{-6}$ GeV $^{-1}$, $B = 10^{13}$ G, $H = 5$ cm, $\theta = 45^\circ$, and $\omega = 1$ keV.

where

$$E_{\perp\pm} = -i \frac{7\hat{q}V\cos\theta}{4\hat{m}u_e^{1/2}\sin^2\theta} E_{\parallel\pm}, \quad (70)$$

with $|E_{\perp\pm}| \ll |E_{\parallel\pm}|$, and

$$\tan 2\theta_m = \frac{4M}{(V - V_{ap})\sin^2\theta}. \quad (71)$$

Again, the above expression reduces to Eq. (46) for $C = 0$. We see that except for the slight shift of the resonance location, $\Delta K = K_+ - K_-$ and θ'_m are the same as those given in Sect. III B, where the coupling with the \perp -mode is neglected. We conclude that the analysis of the axion-photon resonance given in Sect. III B is accurate.

We can similarly show that the vacuum resonance discussed in Sect. III A is hardly affected by the photon-axion coupling.

D. Numerical Examples of Three-Mode Evolution

Here we consider the numerical integration of the axion-photon system in a neutron star atmosphere, with

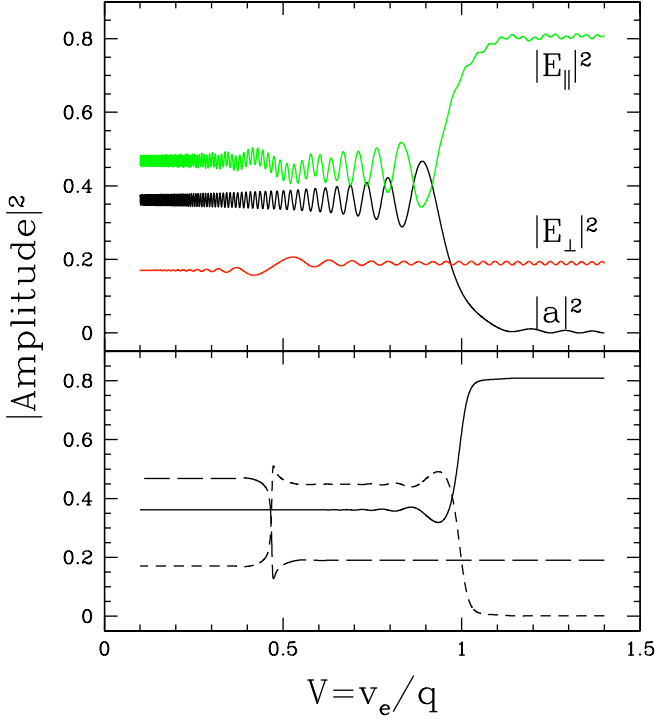


FIG. 11: Same as Fig. 10. except $\omega = 0.3$ keV.

a constant magnetic field \mathbf{B} but varying densities. In our examples, we assume $\rho = \rho_a \exp(-z/H)$, where ρ_a is the density of the axion-photon resonance, and H is the density scale height along the direction of propagation. Equation (39) is equivalent to

$$\frac{d}{dV}\Phi = i \frac{\omega q H}{V} \mathbf{G} \Phi, \quad (72)$$

with \mathbf{G} given by (58). We integrate (72) outward from the high-density region to the low-density region, traversing the axion-photon resonance at $V = 1$ and the vacuum resonance at $V = 1 + m/q$. Fig. 10 and Fig. 11 give two examples of the evolution, with the photon energy $\omega = 1$ keV (Fig. 10) and $\omega = 0.3$ keV (Fig. 11), respectively, both with the parameters $m_a = 10^{-3}$ eV, $g = 10^{-6}$ GeV $^{-1}$, $B = 10^{13}$ G, $H = 5$ cm, and $\theta = 45^\circ$, and the same initial conditions at $V = 1.4$: $E_{\parallel} = 0.9$, $E_{\perp} = \sqrt{0.19}$ and $a = 0$. The lower panels of Figs. 10-11 depict $|A_i|^2$ ($i = 1, 2, 3$), where the mode amplitude A_i is defined by

$$\Phi = \sum_{i=1}^3 A_i \Phi_i, \quad (73)$$

and Φ_i are the normalized mode eigenvectors ($\Phi_i^+ \Phi_i = 1$) discussed in Sect. III C, and $A_i = \Phi_i^+ \Phi$.

The numerical results fully agree with the analytical consideration of Sect. III C, and show that the two resonances can be treated independently of each other. In particular, the mode evolution across the resonance is described by the non-adiabatic jump probability to within

about 30%, Eq. (38) (for vacuum resonance) or (56) (for axion-photon resonance) for values of γ_{res} that vary by nearly seven orders of magnitude from 10^{-6} to 10.

IV. AXION-PHOTON PROPAGATION IN THE SUN AND WHITE DWARFS

The central core of the Sun may a source of keV axions. These axions are the target of the CAST experiment [6]. Could the axions oscillate/transform into photons as they travel across the solar envelope and atmosphere?

The general axion-photon propagation equation (39) can be applied here, and we have $u_e \ll 1$ and Δ_{\parallel} is negligible. As in Sect. III B, it is adequate to consider Eq. (44), with $\Delta_p = -\omega v_e/2 = -\omega_{pe}^2/(2\omega)$. The axion-photon mixing angle is given by [see Eq. (46)]

$$\tan 2\theta_m = \frac{\Delta_M}{(\Delta_a - \Delta_p)/2}. \quad (74)$$

Since $\Delta_M/|\Delta_a| = 5.92 \times 10^{-9} m_{-3}^{-2} g_{-6} \omega_1 B_1 \sin \theta$ (where B_1 is the field strength in units of Gauss, and m_{-3} is the axion mass in units of 10^{-3} eV), we see that the mixing angle is quite small except near the resonance, where $\Delta_p = \Delta_a$. The resonance occurs when $m_a = \omega_{pe}$, at the density $\rho = 1.21 \times 10^{-9} Y_e^{-1} m_{-3}^2$ g cm $^{-3}$, which is outside the photosphere ($\rho \sim 1.6 \times 10^{-7}$ g cm $^{-3}$). At the resonance, the adiabaticity parameter is

$$\gamma_{\text{res}} = \frac{4\Delta_M^2 H}{|\Delta_a|} = 0.042 g_{-6} B_1 \sin \theta \frac{\Delta_M}{|\Delta_a|} \frac{H}{R_{\odot}}, \quad (75)$$

where H is the solar radius. Clearly, $\gamma_{\text{res}} \ll 1$ and no resonant conversion of axion to photon is expected around the resonance.

In the case of magnetic white dwarfs, with B in the range of 10^3 - 10^9 G, we still consider $u_e \ll 1$. The axion-photon resonance is at $v_e = q \sin^2 \theta + (m_a/\omega)^2$, or the density

$$\rho_{\text{res}} = 1.21 \times 10^{-9} Y_e^{-1} m_{-3}^2 (1 + \Delta_{\parallel}/|\Delta_a|) \text{ g cm}^{-3}, \quad (76)$$

where $\Delta_{\parallel}/|\Delta_a| = 0.1855 \omega_1^2 B_9^2 m_{-3}^{-2} \sin^2 \theta$, and $B_9 = B/(10^9$ G). The adiabaticity parameter at the resonance is

$$\begin{aligned} \gamma_{\text{res}} &= \frac{4\Delta_M^2 H}{|\Delta_a|(1 + |\Delta_{\parallel}|/|\Delta_a|)} \\ &= 2.49 \times 10^6 \frac{\omega_1 (m_{-3}^{-1} g_{-6} B_9 \sin \theta)^2}{1 + |\Delta_{\parallel}|/|\Delta_a|} \left(\frac{H}{10^{-2} R_{\odot}} \right) \end{aligned} \quad (77)$$

where we have scaled the density scale height H to the typical radius of the star, $10^{-2} R_{\odot}$. Thus adiabatic resonant axion-photon conversion is a possibility. For a given set of axion parameters, we expect that the flux of photons satisfying $\gamma_{\text{res}} \gg 1$ is reduced by a factor of 2, and significant linear polarization will be present. Observations of the spectra and polarizations of magnetic white

dwarfs would provide constraint on the axion parameters. To carry out such constraint quantitatively, it is necessary to model the low-density region [see Eq. (76)] of the white dwarf atmosphere, a task beyond the scope of our paper.

The evolution of the axion-photon system in the vacuum region outside a white dwarf with a varying magnetic field is similar to the neutron star case studied in Sect. II.

V. DISCUSSION

In this paper we have studied the propagation of the axion-photon system in the atmospheres and the near vicinity of magnetic stars. Because of their strong magnetic fields, we have focused on neutron stars, but our main results/methods can be similarly applied to other astrophysical bodies. Our study goes beyond previous work [11] in that we quantify the various parameter regimes for which axion-photon conversion is important, we calculate the conversion probabilities for propagation in varying magnetic fields and varying plasma densities, and we present examples to illustrate how axion-photon coupling may affect observed photon spectra and polarizations.

The axion-photon resonance (where maximum mixing occurs) is always present in magnetized neutron star atmospheres/magnetospheres. This resonance [see Eq. (43)] is at a higher density than the previously-studied vacuum resonance. Complete axion-photon conversion is possible only when the adiabatic condition [$\gamma_{\text{res}} \gg 1$; see Eq. (52)] is satisfied. A high axion-photon

coupling strength, gradual density gradient and lower photon energy tend to make such conversion a possibility. Note that in this paper we have treated the plasma dielectric tensor in the cold-plasma approximation. For low-energy photons (e.g. optical), the resonance occurs in the neutron star's magnetosphere and the cold plasma treatment is no longer valid. It would be straightforward to generalize our results to more general plasma dielectric tensors.

Even without the axion-photon resonance, partial axion-photon conversion may take place during the propagation in the vacuum region with spatially varying magnetic fields (see Sect. II).

Applying our result to the axions produced at the center of the Sun, we find that there is no possibility for appreciable axion-photon conversion during propagation (see Sect. IV). Our analysis also shows that with the axion parameters allowed by the PVLAS experiment, significant photon-axion resonant conversion is possible in highly magnetized white dwarfs. This may produce interesting spectral and polarization signatures in the observed radiation from the white dwarf.

Acknowledgments

This work was supported in part by NSF grant AST 0307252 and SAO Grant TM6-7004X (DL), as well as a Discovery Grant from NSERC (JSH). This work made use of NASA's Astrophysics Data System. The authors were visitors at the Pacific Institute of Theoretical Physics during the nascent stages of this research.

- [1] R.D. Peccei and H.R. Quinn, Phys. Rev. Lett. **38**, 1440 (1977)
- [2] S. Weinberg, Phys. Rev. Lett. **40**, 223 (1978)
- [3] F. Wilczek, Phys. Rev. Lett. **40**, 279 (1978)
- [4] G.G. Raffelt, Phys. Lett. B **592** (Review of Particle Physics), 391 (2004)
- [5] R. Cameron et al, Phys. Rev. D **47**, 3707 (1993)
- [6] K. Zioutas et al (CAST Collaboration), Phys. Rev. Lett. **94**, 121301 (2005)
- [7] G.G. Raffelt, hep-ph/0504152
- [8] C. Hagmann, K. van Bibber and L.J. Rosenberg, Phys. Lett. B **592** (Review of Particle Physics), 391 (2004), 394 (2004); K. van Bibber and L.J. Rosenberg, Phys. Today. **30**, 28 (2006).
- [9] E. Zavattini et al (PVLAS Collaboration), Phys. Rev. Lett. **96**, 110406 (2006)
- [10] E. Masso and J. Redondo, JCAP, 0509 (2005) 015
- [11] G. Raffelt and L. Stodolsky, Phys. Rev. D **37**, 1237 (1988)
- [12] W. Heisenberg and H. Euler, Z. Physik **98**, 714 (1936).
- [13] J. Schwinger, Phys. Rev. **82**, 664 (1951).
- [14] S.L. Adler, Ann. Phys. **67**, 599 (1971).
- [15] J.S. Heyl and L. Hernquist, J. Phys. A **30**, 6485 (1997).
- [16] A. Y. Potekhin, D. Lai, G. Chabrier and W.C.G. Ho, Astrophys. J., **612**, 1034 (2004)
- [17] D. Lai and W.C.G. Ho, Phys. Rev. Lett. **91**, 071101 (2003)
- [18] M. van Adelsberg and D. Lai, Mon. Not. Roy. Astro. Soc., submitted (2006) (astro-ph/0607168)
- [19] D. Lai and W.C.G. Ho, Astrophys. J. **566**, 373 (2002)
- [20] D. Lai and W.C.G. Ho, Astrophys. J. **588**, 962 (2003)
- [21] W.C.G. Ho and D. Lai, Mon. Not. Roy. Astro. Soc. **338**, 233 (2003)
- [22] Yu.N. Gnedin, G.G. Pavlov and Yu.A. Shibanov, Sov. Astron. Lett. **4**, 117
- [23] P. Meszaros and J. Ventura, Phys. Rev. D **19**, 3565 (1979)
- [24] G.G. Pavlov and Yu.A. Shibanov, Sov. Phys. JETP, **49**, 741 (1979)